ARMY RESEARCH LABORATORY

# Characterization, Processing, and Consolidation of Nanoscale Tungsten Powder

**by Bradley R. Klotz, Franklyn R. Kellogg, Eric M. Klier, Robert J. Dowding, and Kyu C. Cho**

**ARL-TR-5045** **December 2009**

## NOTICES

### Disclaimers

The findings in this report are not to be construed as an official Department of the Army position unless so designated by other authorized documents.

Citation of manufacturer's or trade names does not constitute an official endorsement or approval of the use thereof.

Destroy this report when it is no longer needed.  Do not return it to the originator.

**Army Research Laboratory**
Aberdeen Proving Ground, MD 21005-5069

**ARL-TR-5045** **December 2009**

# Characterization, Processing, and Consolidation of Nanoscale Tungsten Powder

**Bradley R. Klotz**
**Dynamic Science, Inc.**

**Franklyn R. Kellogg**
**Data Matrix Solutions**

**Eric M. Klier, Robert J. Dowding, and Kyu C. Cho**
**Weapons and Materials Research Directorate, ARL**

| REPORT DOCUMENTATION PAGE | Form Approved OMB No. 0704-0188 |
|---|---|



| 1. REPORT DATE *(DD-MM-YYYY)* | 2. REPORT TYPE | 3. DATES COVERED (From - To) |
|---|---|---|
| December 2009 | Final | March 2005–March 2008 |

**4. TITLE AND SUBTITLE**
Characterization, Processing, and Consolidation of Nanoscale Tungsten Powder

**5a. CONTRACT NUMBER**

**5b. GRANT NUMBER**

**5c. PROGRAM ELEMENT NUMBER**

**6. AUTHOR(S)**
Bradley R. Klotz,[*] Franklyn R. Kellogg,[†] Eric M. Klier, Robert J. Dowding, and Kyu C. Cho

**5d. PROJECT NUMBER**
1L162618AH80

**5e. TASK NUMBER**

**5f. WORK UNIT NUMBER**

**7. PERFORMING ORGANIZATION NAME(S) AND ADDRESS(ES)**
U.S. Army Research Laboratory
ATTN: RDRL-WMM-B
Aberdeen Proving Ground, MD 21005-5069

**8. PERFORMING ORGANIZATION REPORT NUMBER**
ARL-TR-5045

**9. SPONSORING/MONITORING AGENCY NAME(S) AND ADDRESS(ES)**

**10. SPONSOR/MONITOR'S ACRONYM(S)**

**11. SPONSOR/MONITOR'S REPORT NUMBER(S)**

**12. DISTRIBUTION/AVAILABILITY STATEMENT**
Approved for public release; distribution is unlimited.

**13. SUPPLEMENTARY NOTES**
[*]Dynamic Science, Inc., Aberdeen Proving Ground, MD 21005-5069
[†]Data Matrix Solutions, Aberdeen Proving Ground, MD 21005-5069

**14. ABSTRACT**
Nanoscale tungsten powder was consolidated by the Plasma Pressure Compaction ($P^2C$) method. The starting powder was first characterized to determine particle size, morphology, and presence of chemical impurities. The characterization data led to efforts to deagglomerate the as-received powder through milling and experiments into hydrogen reduction of oxygen present in the powder. After consolidation, densities of the resulting samples were measured, microstructural features (including grain size) were examined, and chemical analysis was carried out to detect the presence of impurities. The study concluded that it was possible to consolidate the nanocrystalline powder and maintain nano-sized grains. However, retention of initial grain size came at the expense of sample density.

**15. SUBJECT TERMS**
tungsten, nanomaterials, powder consolidation

| 16. SECURITY CLASSIFICATION OF: | | | 17. LIMITATION OF ABSTRACT | 18. NUMBER OF PAGES | 19a. NAME OF RESPONSIBLE PERSON |
|---|---|---|---|---|---|
| a. REPORT | b. ABSTRACT | c. THIS PAGE | | | Bradley R. Klotz |
| Unclassified | Unclassified | Unclassified | UU | 38 | 19b. TELEPHONE NUMBER (*Include area code*) 410-306-2130 |

**Standard Form 298 (Rev. 8/98)**
Prescribed by ANSI Std. Z39.18

## Contents

## List of Figures

## List of Tables

## Acknowledgments

This research was supported in part by an appointment to the research participation program at the U.S. Army Research Laboratory (ARL) administered by the Oak Ridge Institute for Science and Education through an interagency agreement between the U.S. Department of Energy and ARL.

# 1. Introduction

The high density of tungsten (W) makes it desirable for use in anti-armor applications, in particular as a replacement material for depleted uranium (DU) in kinetic energy (KE) penetrators. Unstable plastic deformation and flow softening of DU produce shear localization in the form of adiabatic shear bands in the KE penetrator upon impact, resulting in the formation of a chisel-nose on the penetrator tip and enhanced penetration performance (*1*). The tendency of conventional grain size W to exhibit plastic stability and resistance to flow localization limits its applicability in these areas (*2*). However, it has been shown that when tungsten grains are refined to 500 nm or less by severe plastic deformation techniques, significant flow localization is exhibited and strain rate sensitivity is reduced (*3*). Furthermore, for W with grain sizes of ~100 nm produced by high pressure torsion, localized shearing is observed (*4*). Thus, it is possible that W with grain sizes in the nano-crystalline (<100 nm) or ultra-fine grain (<500 nm) regime could exhibit the failure behavior required for use in anti-armor applications.

The consolidation of nano-sized tungsten powder is one method of producing bulk nanocrystalline parts. A requirement for this approach is the ability to obtain large quantities of good quality tungsten nanopowder that can then be consolidated by a densification technique that will produce a part with high density while retaining the initial grain size. Densification behavior of tungsten nanopowder is reliant on the properties of the initial powder, such as chemical purity, particle size, size distribution, morphology, and degree of agglomeration. Detailed characterization of starting powder is therefore important to assess its suitability for use in the production of bulk tungsten parts. Furthermore, efforts have already been undertaken at the U.S. Army Research Laboratory (ARL) to consolidate fine-grained tungsten by the Plasma Pressure Compaction ($P^2C$) method (*5*). The $P^2C$ process works by subjecting a powder sample to an electrical current with very high amperage, enabling rapid heating rates and very short high temperature soak times which could result in rapid consolidation with little grain growth. The previous studies showed that submicron tungsten powder could be consolidated by $P^2C$ to 97% theoretical density. However, the final grain size of the samples was approximately ten times larger than the initial powder size. Perhaps the use of nanocrystalline tungsten powders could provide for a sample with final grain size in the nanocrystalline or ultra-fine grain regime.

A purportedly nanocrystalline tungsten powder has become commercially available. The following report details efforts to evaluate this tungsten powder for use in the consolidation of bulk nanocrystalline samples. Particle size, morphology, degree of agglomeration, and chemical purity of the starting powder were examined using a variety of powder characterization techniques. Several different methods of treating the powder prior to consolidation were also undertaken to improve suitability of the powder for the production of high density samples.

Consolidation of the powder was carried out by the $P^2C$ method, and resulting samples were examined to evaluate properties such as density, grain size, and chemical purity.

## 2. Experimental Procedure

Approximately 25 kg of the nanocrystalline tungsten powder were obtained. A particle size of 45 nm was calculated for the powder using the vendor-supplied BET surface area value of 6.86 $m^2/g$. The size and morphology of the as-received powder were observed on a Hitachi S-4700 Field Emission Scanning Electron Microscope (FESEM) with energy dispersive x-ray spectroscopy (EDS) capabilities. Surface area of the powder was measured on a Micromeritics ASAP 2000 Brunauer, Emmet, and Teller (BET) Surface Area Analyzer. Samples of the powder were also dispersed in a water-glycerol mixture, and the particle size distribution (PSD) was determined by laser scattering techniques on both a Horiba LA-910 Laser Scattering Particle Size Distribution Analyzer and a Horiba LB-500 Dynamic Light Scattering Particle Size Analyzer. Elemental chemical analysis of the powder was carried out for ARL by Luvak, Inc. of Boylston, MA, and the results were compared to those provided by the manufacturer, as well as measurement data provided by Kennametal, Inc of Latrobe, PA. In addition, an x-ray diffraction (XRD) pattern to detect the presence of impurity phases in the powder was generated on a Phillips X-Ray Diffractometer with Phillips X-Pert Analysis software.

Both electron microscopy and PSD measurement showed that the powder consisted of very large agglomerates of fine powder. To break up these agglomerates, a rudimentary milling procedure was applied. Different milling conditions were used in an effort to determine the best milling parameters. For the first experiment, 100 g of tungsten powder was placed in a 250-mL tungsten carbide jar with 50 10-mm diameter tungsten carbide balls and milled on a Retsch Type PM 400 Planetary Ball Mill at 200 RPM for 8 h. A small amount of powder was removed from the jar after 1, 2, and 4 h to observe the effect of milling time on particle size. Additional samples of powder were also milled with 25 and 75 balls to examine the effect of amount of milling media, as well as at speeds of 100 and 300 RPM to examine the effect of mill speed. Milled powder was characterized using the same techniques detailed for the starting powder, including chemical analysis after milling to determine if any impurities were introduced through the milling process.

After chemical analysis detected the presence of a large amount of oxygen in both the starting and milled powders, experiments on hydrogen reduction of the powder were carried out by heating samples of the powder in a tube furnace under hydrogen atmosphere. Surface area of the reduced powder samples was measured by the BET method to determine whether sintering of the

nanopowders had occurred during the reduction process. The presence of oxide phases could also result in the starting powder having a density lower than that of pure tungsten. Thus, a Micromeritics AccuPyc 1330 helium pycnometer was used to measure the density of the powder. The principle used in helium pycnometry is the same as Archimedes' method for density determination, except water is replaced with helium gas, making it possible to accurately determine densities of powders. The tungsten powders were loaded into a 10 $cm^3$ aluminum cylinder and placed in the pycnometer. The powder was tested in three conditions: as received powder, as received powder that was baked overnight at 120 °C to drive off absorbed moisture, and powder that was planetary milled and baked over night at 115 °C. Pycnometer testing was repeated until the results were reproducible (based upon the size of the standard deviations).

The development of $P^2C$ processing parameters for tungsten have been described previously (*5–6*). For this study, 30–50 g of W powder were packed into 1-in-diameter graphite dies and placed between two water cooled platens in the chamber of the $P^2C$ apparatus (figure 1). Samples were loaded at a pressure of 22 MPa. Prior to consolidation, the chamber was pumped down to 10 millitorr or less. All consolidation runs were carried out under vacuum, and certain samples were also pre-treated in the $P^2C$ chamber under hydrogen. The samples were first subjected to a pulsed current with 10-μs on/off times. Pulsed currents of 200, 400, 600, 800, and 1000 A were applied in a step-wise fashion with 5-min intervals at each pulsing step. The temperature of the sample was monitored at the outside surface of the die with an optical pyrometer, which did not register a temperature until the die wall reached 636 °C. The powder compact itself inside the die has been shown to be at a much higher temperature (*7*). The pulsing parameters were run until the pyrometer started to read a temperature. For most samples, this occurred after being at 1000 A for 5 min. Once the pyrometer became active, the pressure was increased to 100 MPa, the power supply was switched to constant current mode, and the current was rapidly increased to 5000 A. The applied current of 5000 A was maintained until the sintering temperature was reached, at which point the current was rapidly lowered to zero, providing for a dwell time at temperature of essentially 0. The sample was then allowed to cool under vacuum.

For samples which underwent hydrogen pre-treatment, the powder was placed in a graphite die and loaded into the $P^2C$. The sample was then held at 22 MPa inside the $P^2C$ apparatus at a chamber pressure of ~5 psi under a constant flow of hydrogen and heated by graphite resistance heaters in the chamber. A small hole was drilled into the graphite die and a thermocouple was inserted to measure the temperature of the sample. This thermocouple was then used to control the temperature of the resistance heaters. Samples were heated under hydrogen to the desired temperature and held there for a set time, in this case 380 min. After reduction, the chamber was backfilled with argon and then pumped down to a vacuum level of 5 millitorr before the consolidation was performed as detailed previously.

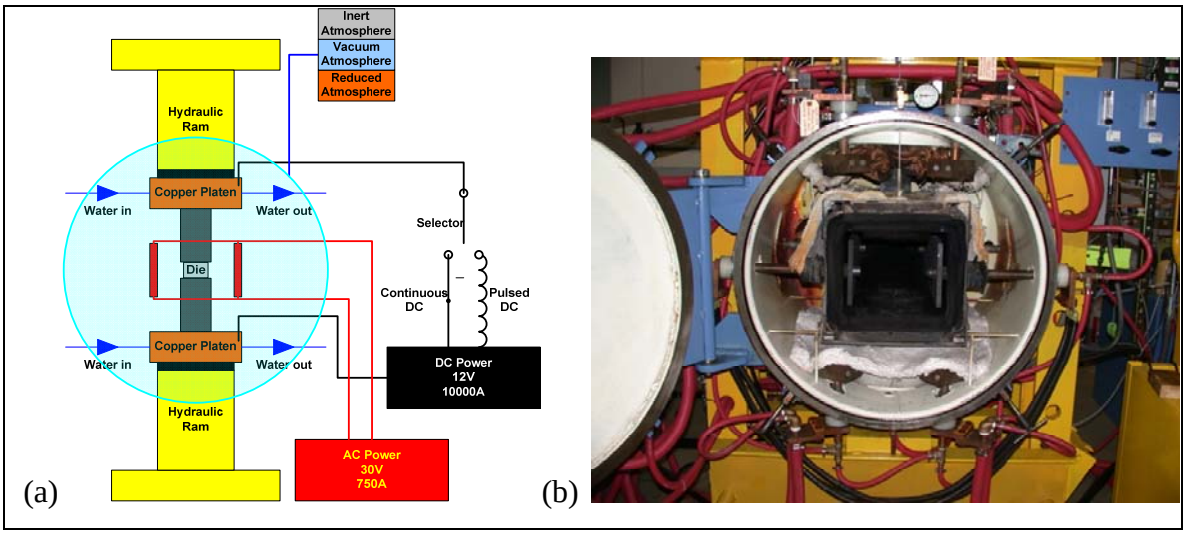


Figure 1. The $P^2C$ apparatus: (a) schematic and (b) photograph of sample chamber.

After consolidation, samples were ground to remove graphite or tungsten carbide on the surface, and density was measured by Archimedes' method. Samples were then sectioned perpendicular to the pressing direction to provide specimens for scanning electron microscopy and chemical analysis.

## 3. Results and Discussion

FESEM micrographs of the as-received tungsten powder are shown in figure 2. The lower-magnification micrographs show very large, rectangular prism-shaped aggregates, some as large as 10–20 μm. Higher magnification images show these large aggregates to be comprised of individual fine particles on the order of 100–200 nm that are joined together. These large "hard" agglomerates of solidly joined particles will most likely need to be broken up to enhance the sinterability of the starting powder. The nature of the joining between the particles means that some sort of mechanical milling procedure will have to be performed to break the larger aggregates down to the individual fine particles.

BET surface area values for the powder measured at ARL, as well as those obtained from the vendor and Kennametal, Inc., are shown in table 1. The three measurements were relatively close to each other, with the ARL-generated value showing the highest surface area at 5.17 $m^2/g$. Back-calculating for a particle diameter using each BET surface area values resulted in a particle diameter range of 40–60 nm for the three measurements. All three values were lower than the 100–200 nm value for the individual particles estimated from the FESEM photos, but the nature of the agglomeration in the powder makes getting accurate particle diameter values from surface area values difficult.

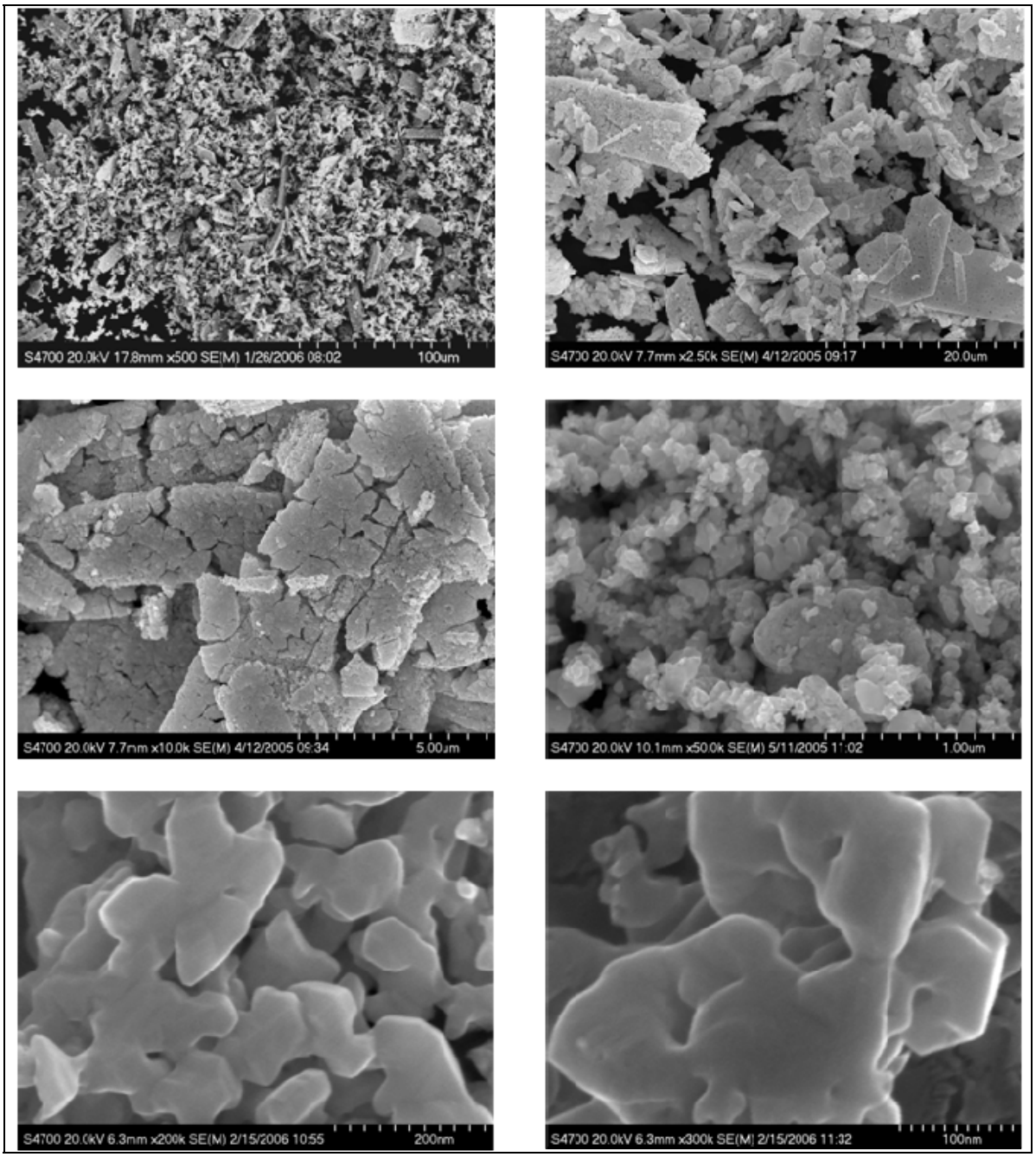


Figure 2. FESEM images of as-received tungsten powder.

Table 1. BET surface area values.

| | **Vendor Supplied** | **Kennametal Measured** | **ARL Measured** |
|---|---|---|---|
| BET surface area | 6.86 $m^2/g$ | 7.78 $m^2/g$ | 5.17 $m^2/g$ |
| Particle diameter | 45 nm | 40 nm | 60 nm |

Particle size distribution plots of the as-received powder obtained from both the Horiba LA-910 and LB-500 instruments are shown in figure 3. The LA-910 is able to detect a large range of particle sizes, so it is able to distinguish the large agglomerates observed by FESEM as evidenced by the peak centered at ~10 μm. The plot also shows that the powder contains particles with sizes as small as ~500 nm. The LB-500 has a much smaller range of particle size detection capabilities and is more suited to detecting very fine particles. The sample of ZY powder was shown to have fine particles with a size range centered between 400 and 500 nm, with some particles as small as 200 nm present. The generated distributions appeared to agree with the size of the particles observed by FESEM.

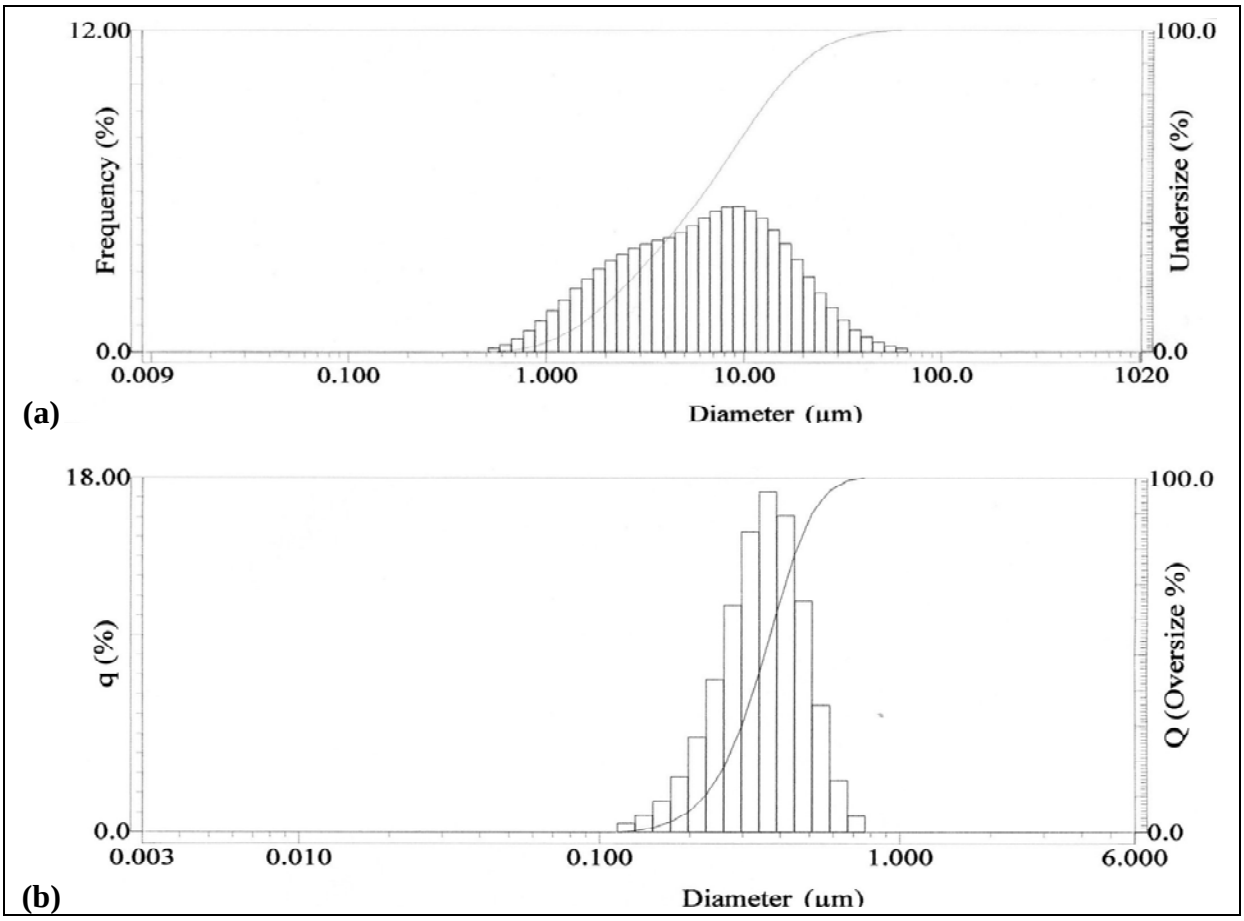


Figure 3. Particle size distributions for as-received tungsten powder as measured on the (a) Horiba LA-910 and (b) Horiba LB-500.

The results of chemical analysis of the tungsten powder are shown in table 2. The amount of sulfur and carbon were determined by combustion infrared detection, oxygen content was measured by inert gas fusion, and all other elements were measured by direct current plasma emission spectroscopy. The analysis showed a relatively high amount of oxygen in the powder. As a result of the high oxygen content, powder reduction experiments were undertaken.

Table 2. Elemental analysis of tungsten powder.

| Element | Vendor Supplied (Weight-Percent) | Kennametal Measured (Weight-Percent) | ARL Measured (Weight-Percent) |
|---|---|---|---|
| Al | <0.0005 | — | <0.0005 |
| As | <0.0008 | — | <0.0020 |
| Bi | <0.0001 | — | <0.0020 |
| C | not supplied | <0.01 | 0.029 |
| Ca | 0.0010 | — | 0.0010 |
| Cd | <0.0001 | — | <0.0005 |
| Co | <0.0005 | — | <0.0005 |
| Cr | 0.0013 | — | <0.0005 |
| Cu | 0.0001 | — | <0.0005 |
| Fe | 0.0039 | <0.025 | 0.0026 |
| K | 0.0013 | — | <0.0005 |
| Mg | <0.0003 | — | <0.0005 |
| Mn | <0.0005 | — | <0.0005 |
| Mo | 0.0015 | — | 0.0020 |
| Na | 0.0025 | — | 0.0032 |
| Ni | 0.0007 | <0.025 | 0.0021 |
| O | 0.9400 | 0.98 | 1.40 |
| P | 0.0005 | — | <0.0020 |
| Pb | <0.0001 | — | <0.0010 |
| S | 0.0017 | — | 0.0025 |
| Sb | <0.0006 | — | <0.0020 |
| Si | 0.0028 | — | 0.0023 |
| Sn | 0.0004 | — | <0.0020 |
| Ti | <0.0005 | — | <0.0005 |
| V | <0.0005 | <0.025 | <0.0005 |

An XRD pattern for the powder is shown in figure 4. No significant amounts of other phases were detected, as only peaks corresponding to tungsten were shown. The large amount of oxygen detected in the powder by chemical analysis could therefore be present as elemental oxygen on the surface of the powders. If tungsten oxide phases are present, the quantity was not significant enough to be detected by XRD.

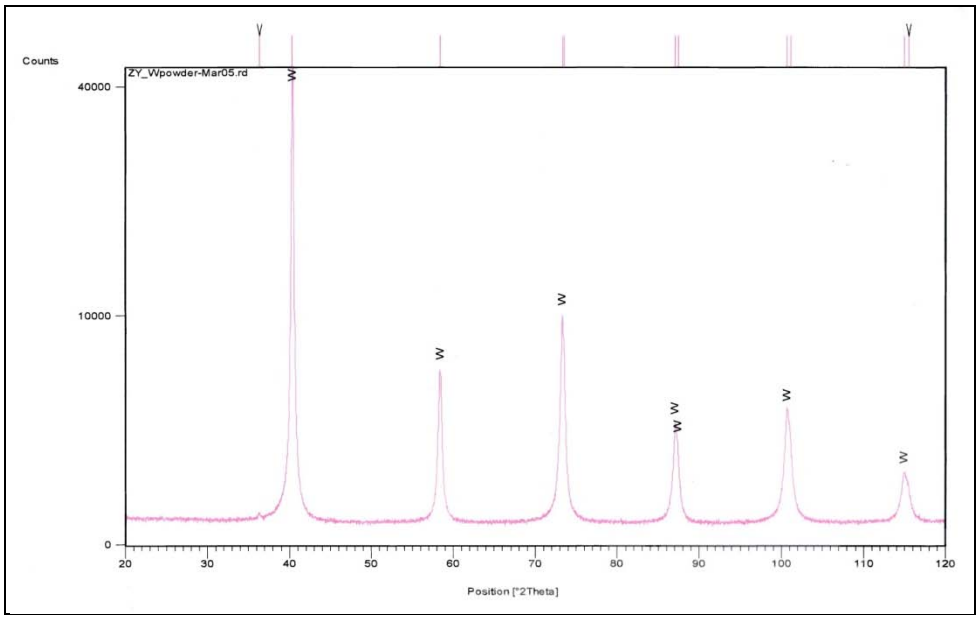


Figure 4. X-ray diffraction pattern for as-received tungsten powder.

Based on the results of the FESEM and particle size distribution analyses, planetary ball milling of the as-received powder was performed to try and obtain a starting powder with the finest particle size possible. After 1 h of milling, the rectangular agglomerates were seen to be mostly broken up, but the powder was still highly agglomerated (figure 5). Further milling up to 8 h did not appear to change the appearance of the powder. Milling the powder for 1 h with different amounts of milling media (figure 6) and at different RPMs (figure 7) also appeared to be effective in breaking up the initial agglomerates. However, from FESEM observations alone, it is not clear enough to determine which set of milling parameters did the best job of breaking down the powders. Particle size distribution analysis was also performed to better reveal the changes in the particle size of the powder achieved through planetary milling, and to determine which combination of milling parameters is best for achieving powder in the most desirable condition for consolidation.

As with the starting powder, the particle size distribution of the milled powders was measured using two different laser light scattering methods. Plots of particle size distribution as determined by the Horiba LA-910 particle size analyzer for two samples of the milled powder, as well as a plot of the as-received powder for comparison, are shown in figure 8. Many of the large aggregates appeared to be broken up after 1 h of milling with 50 balls at 200 RPM, as evidenced by the formation of a peak at around 500–600 nm and a shift of the low end of the distribution to ~100 nm (figure 8b). The peaks at higher particle size still present for the milled sample could either be due to some large aggregates still remaining after milling or the formation of agglomerates of fine particles as observed in the FESEM images. Milling for longer than 1 h with the same mill speed and media did not appear to further reduce the size of the finest particles or completely remove the large agglomerates (figure 8c).

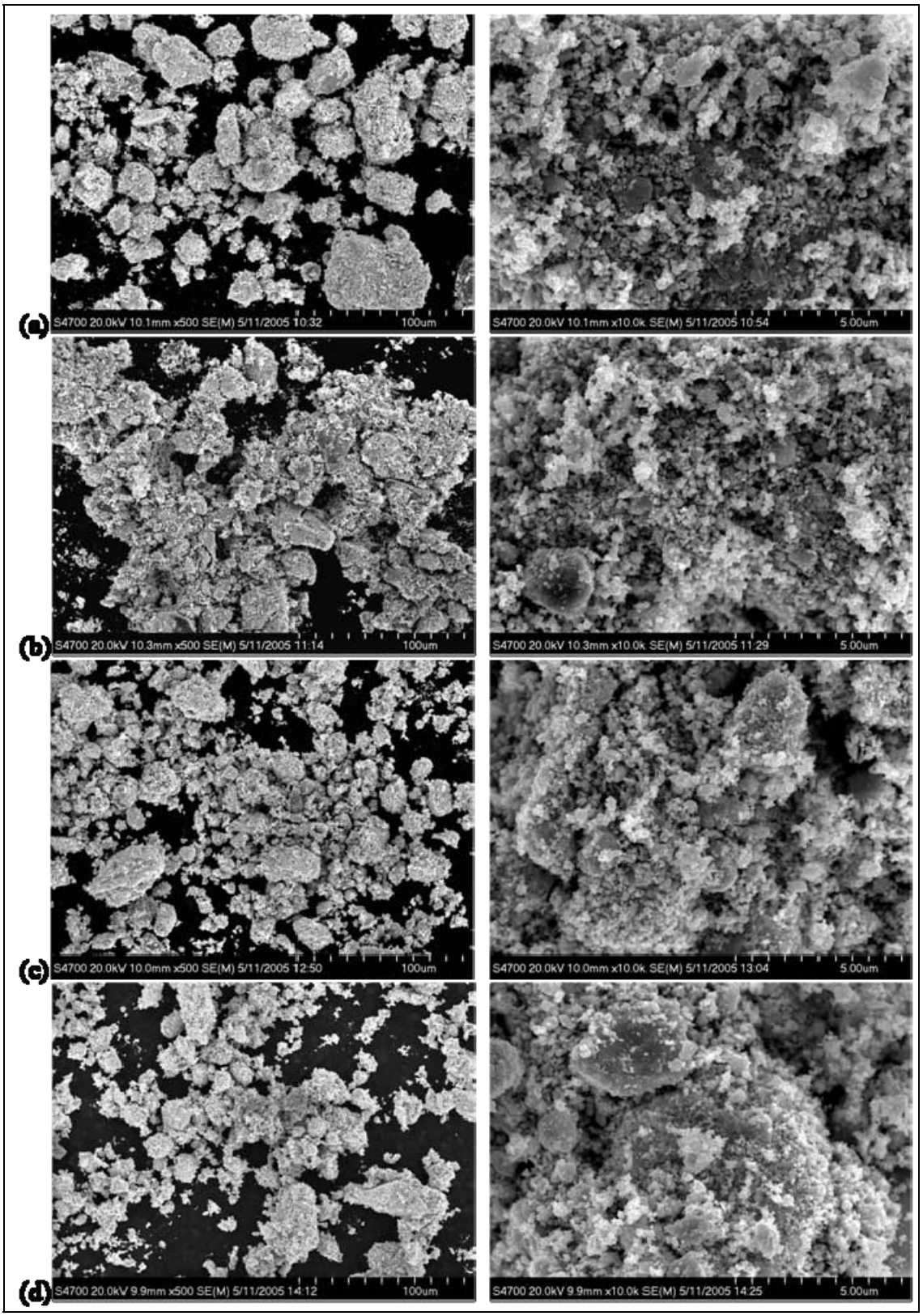


Figure 5. Micrographs showing the effects of milling time. Samples were milled with 50 pellets at 200 RPM for (a) 1, (b) 2, (c) 4, and (d) 8 h.

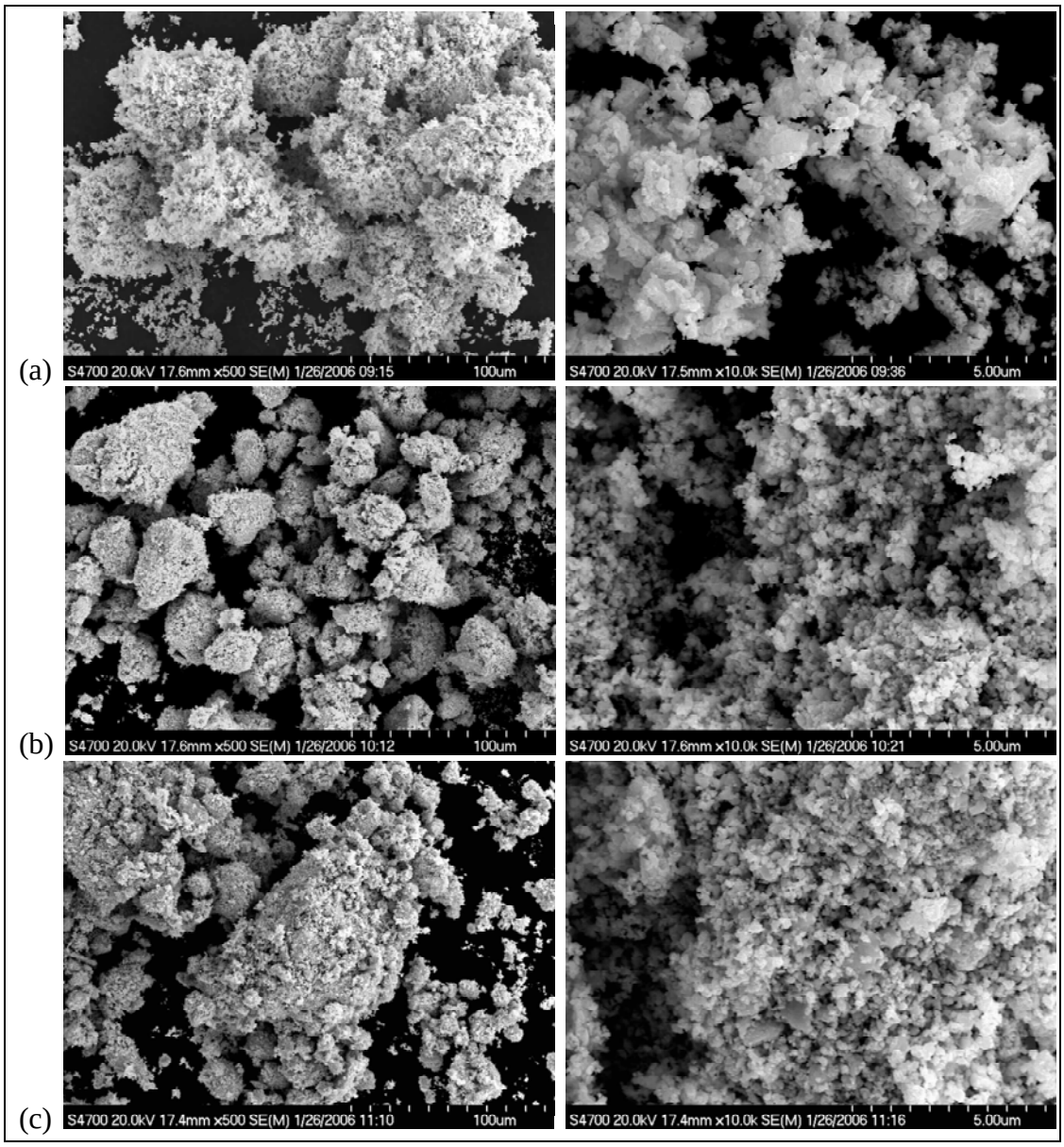


Figure 6. Micrographs showing the effects of the number of milling pellets used. All samples were milled for 1 h at 200 RPM with (a) 25 10-mm tungsten carbide balls, (b) 50 10-mm tungsten carbide balls, and (c) 75 10-mm tungsten carbide balls.

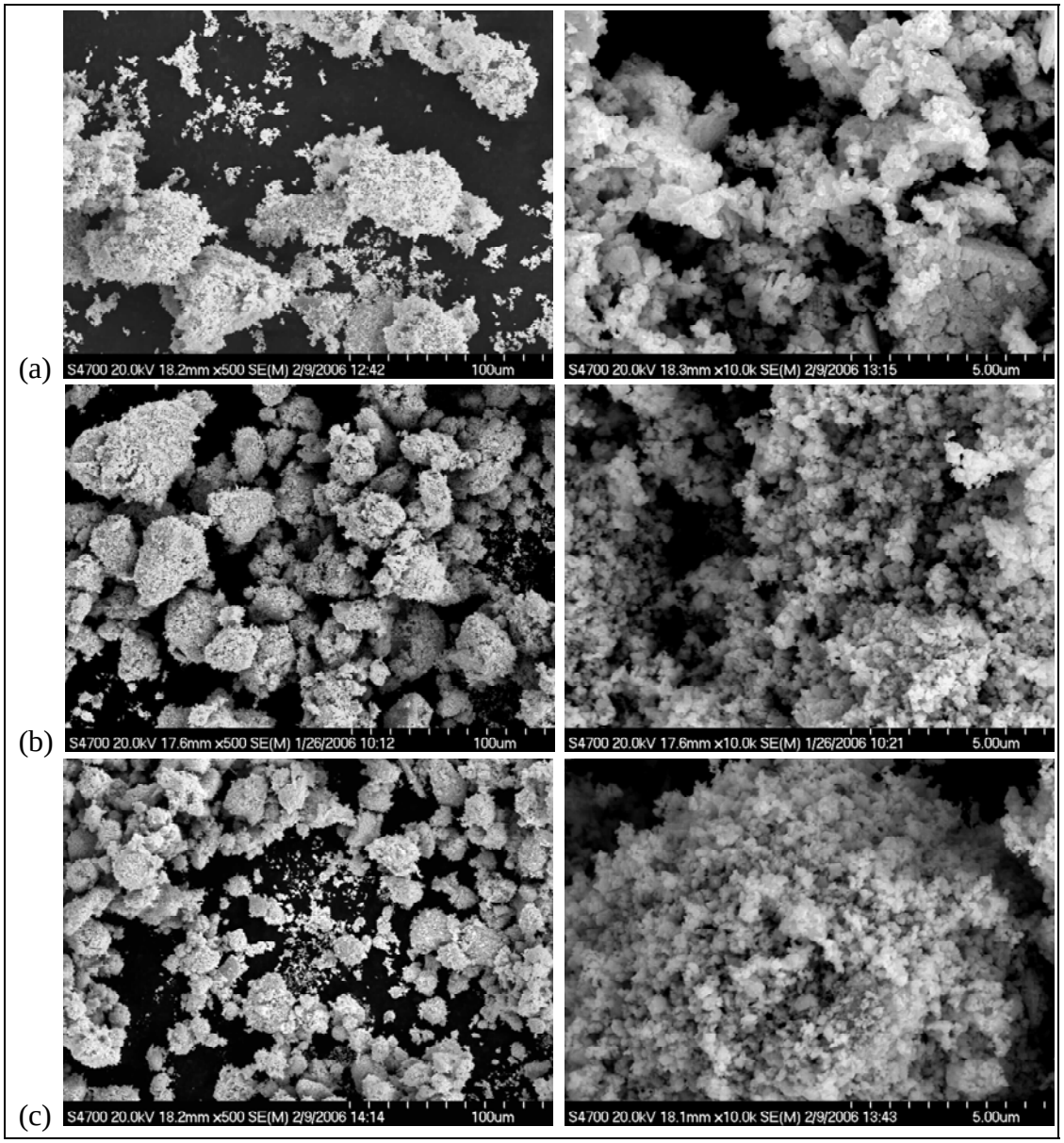


Figure 7. Micrographs showing the effects of milling RPM on powder. All samples were milled with 50 pellets for 1 h at (a) 100, (b) 200, and (c) 300 RPM.

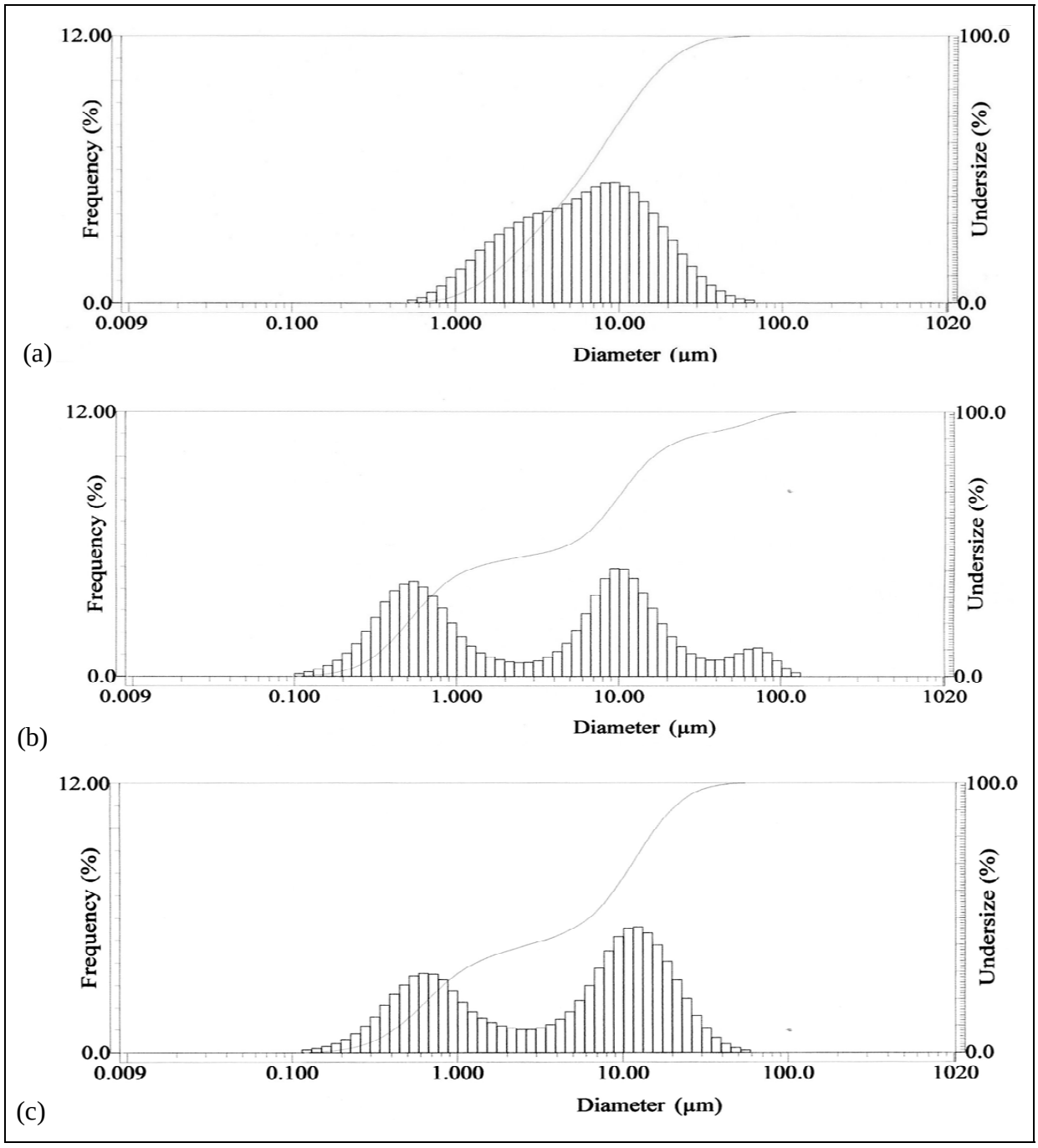


Figure 8. Particle size distribution plots for (a) unmilled powder, (b) powder milled 1 h with 50 balls at 200 RPM, and (c) powder milled 2 h with 50 balls at 200 RPM.

Data generated by the LB-500 dynamic light scattering method, which is able to better measure very fine particles, showed that there was a significant reduction in mean particle size of the fine particles in all the milled samples compared to the as-received powder. Mean particle size was seen to decrease most dramatically after 1 h of milling and changed very little as milling time increased (figure 9). The data also showed that using 50 balls reduced the average particle size more than when 25 or 75 balls were used (figure 10). It is believed that using 75 pellets caused the particles to re-agglomerate, leading to a larger mean particle size. The RPM at which the mill is operated was also seen to have a large effect on particle size (figure 11). The mean particle size when running at 300 RPM was reduced from ~440 to ~74 nm, which was slightly lower than the ~88 nm size achieved when 200 RPM was used. At 100 RPM, the mean particle size decreased only to ~260 nm, showing that there is insufficient energy in the system to accomplish a significant decrease in particle size at that speed. Thus, the particle size distribution data collected suggests that the best milling procedure was 1 h of milling at 300 RPM with 50 balls. However, the milling jar was found to be too hot to handle immediately after milling at 300 RPM, and, after cooling, the jar expelled gas laced with tungsten particles into the air when opened. This made it undesirable to utilize the 300 RPM mill speed.

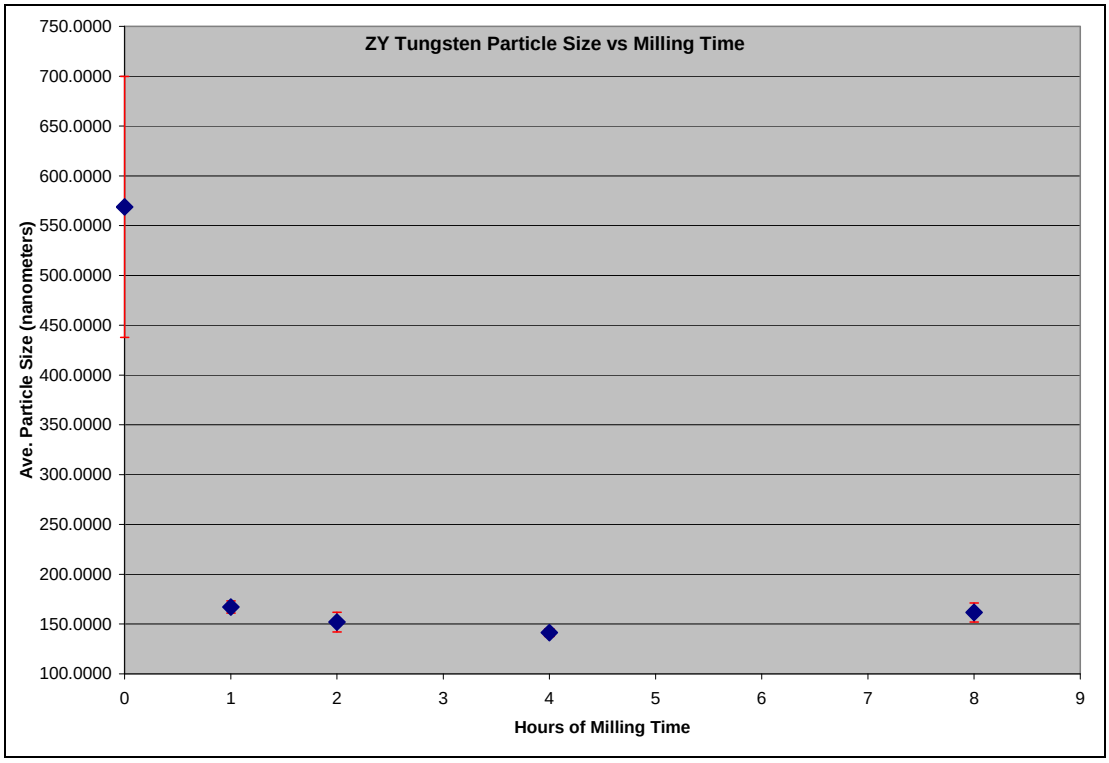


Figure 9. Plot of mean particle size vs. milling time.

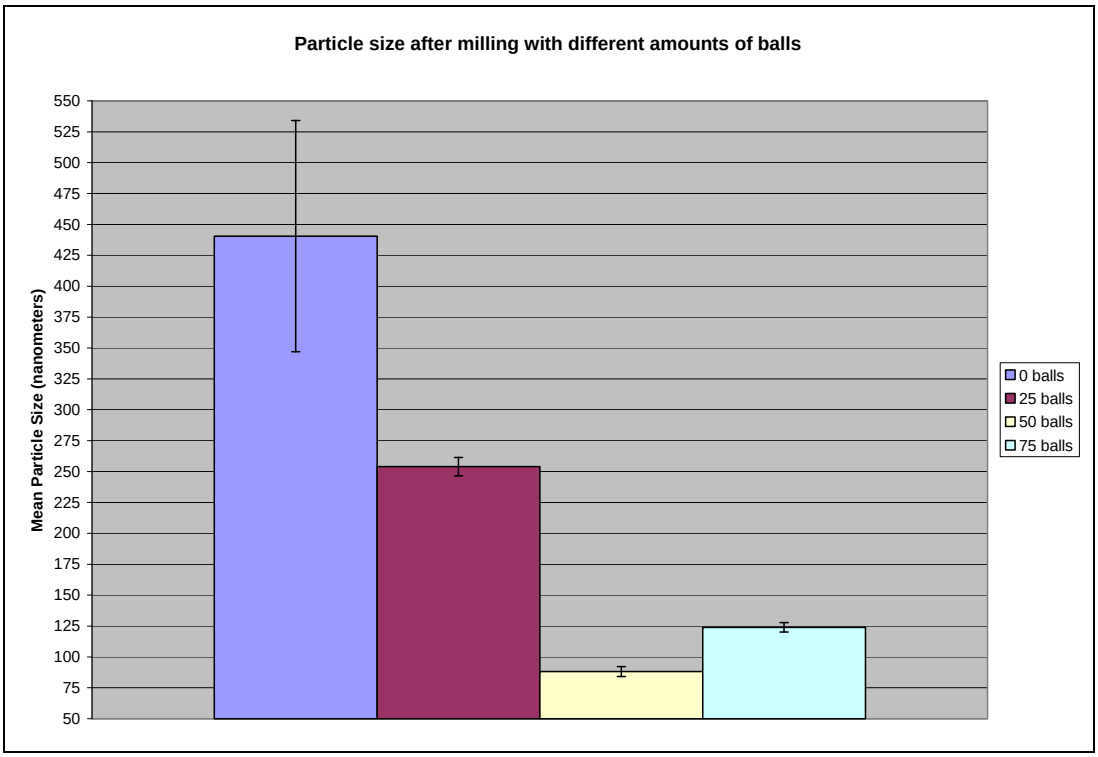


Figure 10. Graph of mean particle size change with amount of milling media.

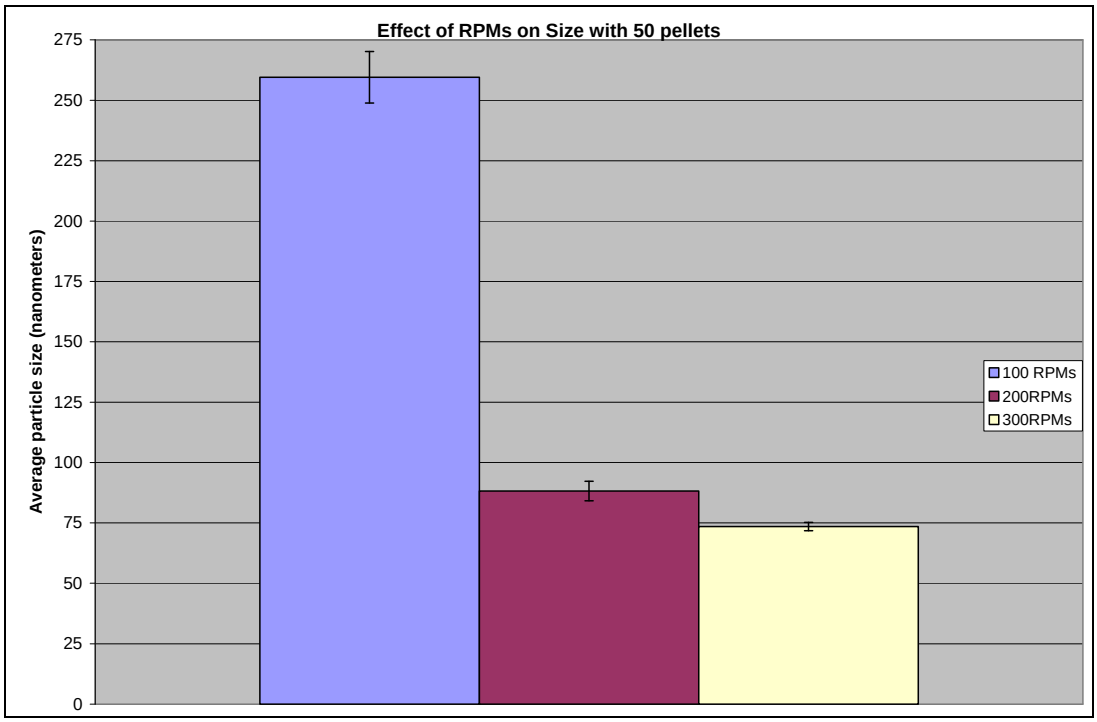


Figure 11. Graph of mean particle size change with mill RPM.

Powder samples were sent for chemical analysis to attempt to detect contamination from the tungsten carbide milling media and any further oxygen picked up by the powder during the milling process. Carbon was tested for via combustion infrared detection, cobalt content was measured by direct current plasma emission spectroscopy, and oxygen was detected by inert gas fusion. The results show that carbon and cobalt levels did not change very much during milling, while oxygen levels were seen to increase (table 3). The data shows that the most effective milling procedure (50 balls for 1 h at 300 RPM) led to an increase in oxygen content from 1.4 weight-percent oxygen in the as-received powder to ~1.78 weight-percent in the milled specimens. Using 50 balls for 1 h at 200 RPM led to an increase from 1.4 to 1.74 weight-percent oxygen. Since the use of both 200 and 300 RPM mill speeds produced samples with a similar increase in oxygen content, as well as similar average particle sizes, it was chosen to mill the powder using 50 balls for 1 h at 200 RPM, due to the fact that handling the milling jar afterward was safer and easier than when running at the higher speed.

Table 3. Chemical analysis of milled tungsten powders.

| **Milling Conditions** | **Carbon (Weight-Percent)** | **Oxygen (Weight-Percent)** | **Cobalt (Weight-Percent)** |
|---|---|---|---|
| Un-milled | 0.029 | 1.40 | 0.010 |
| 25 balls, 200 RPM | 0.024 | 1.47 | 0.010 |
| 50 balls, 200 RPM | 0.026 | 1.74 | 0.0070 |
| 75 balls, 200 RPM | 0.026 | 1.81 | 0.0078 |
| 50 pellets, 100 RPM | 0.025 | 1.49 | 0.0092 |
| 50 pellets, 300 RPM | 0.029 | 1.78 | 0.0083 |

The presence of oxygen in the powder both before and after milling made it necessary to reduce the powder under a hydrogen atmosphere prior to compaction. A reduction time and temperature combination needed to be determined that would allow for adequate reduction of the oxygen in the powder without causing any additional agglomeration or sintering of the particles. Green bodies were made by pressing 25 g of milled tungsten powder to 4 ton in a 1-in stainless steel die. A control sample of as-received powder was also pressed. The green bodies would then be placed in a tube furnace and heated under hydrogen. In previous work with larger grained tungsten powder, it was determined that the best method for tungsten reduction was to place the powder in a flat alumina boat in a tube furnace and soak at 850 °C for 2 h under hydrogen (*5*). Thus, the first compact was heated to 850 °C and held for 2 h in a hydrogen atmosphere. The results of BET surface area measurement of the reduced samples are shown in table 4. The specimen reduced at 850 °C showed a decrease in surface area when compared with an unheated compact, indicating that sintering of the tungsten particles may have occurred during the reduction process. The decision was made to reduce the temperature to 750 °C while keeping the hold time the same. The first sample made at 750 °C spontaneously reacted when it was Table 4. BET surface area measurements for hydrogen reduced samples.

| Reduction Temperature (°C) | Reduction Time (min) | BET Surface Area ($m^2/g$) |
|---|---|---|
| unheated | 0 | 5.1677 ± 0.0786 |
| 850 | 120 | 3.5352 ± 0.0407 |
| 750 | 120 | 4.6788 ± 0.0462 |
| 650 | 380 | 5.3574 ± 0.0681 |

pulled from the furnace. It changed color from purple to brown, then to orange and yellow, finally ending up as a bluish-green pile of ash. XRD confirmed that several different tungsten oxides were present in this ash. A second compact run under the exact same parameters survived the heating cycle and was removed from the furnace intact. For the sample reduced at 750 °C that survived the furnace treatment, the BET measurements also showed a slight decrease in surface area. The experiment was repeated at 650 °C for 2 h. Two samples made at this temperature also reacted upon removal from the furnace to became tungsten oxide. At first, it was assumed that this reaction was being fueled by residual water and oxygen in the sample due to incomplete reduction. A more likely explanation is that the samples reacted due to the fact that the tungsten oxide present in the powders, which acted as a passivation layer, had been removed, and the particles had not sintered enough to overcome the reactivity that nano-sized particles often have due to their high surface area. The samples treated at the higher temperatures did not react because either they had sintered enough to increase their surface area, or there was still enough tungsten oxide present to act as a passivating layer.

In order to determine which set of time and temperature parameters would not result in spontaneous reactions, an empirical formula developed from industrial processes used to reduce tungsten oxide to tungsten powder was used to calculate the required reduction times at lower temperatures (*8*). The equation is:

$$t = (6.66*10^{20})\rho\, T^{-5.7}(f\, h)^{1.6}, \quad (1)$$

where t is the reduction time (seconds), ρ is the bulk density of oxide (grams per cubic centimeter), T is the reduction temperature in Kelvin, f is the fraction of oxide reduced, and h is the bed depth in centimeters. This formula is not an exact fit for this experiment because it assumes that the starting powder is tungsten oxide, whereas in this case the starting powder is tungsten with 1.4 weight-percent oxygen. By assuming that the 2-h reduction at 850 °C leads to a fully reduced sample, and by using the same alumina boat and green body size for each experiment, it is possible to combine the unknown variables (ρ, f, and h) and solve for them figure 12 shows a plot of reduction temperature vs. time required to fully reduce a tungsten sample. Following these results, a sample was reduced under hydrogen at 650 °C for 6 h and 20 min. It survived the reduction process and showed a BET surface area very similar to the unreduced green body sample (see table 4). FESEM micrographs of the reduced tungsten compacts are shown in figure 13. Evidence of particle coalescence and sintering can be seen in the 850 °C sample, while the 650 and 750 °C samples appear similar to the unheated sample.

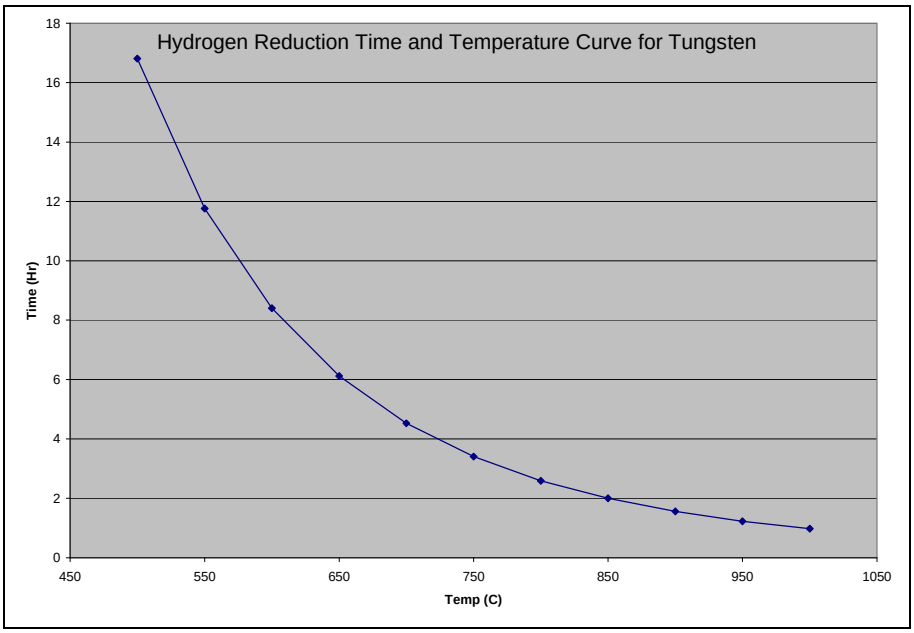


Figure 12. Hydrogen reduction curve for tungsten.

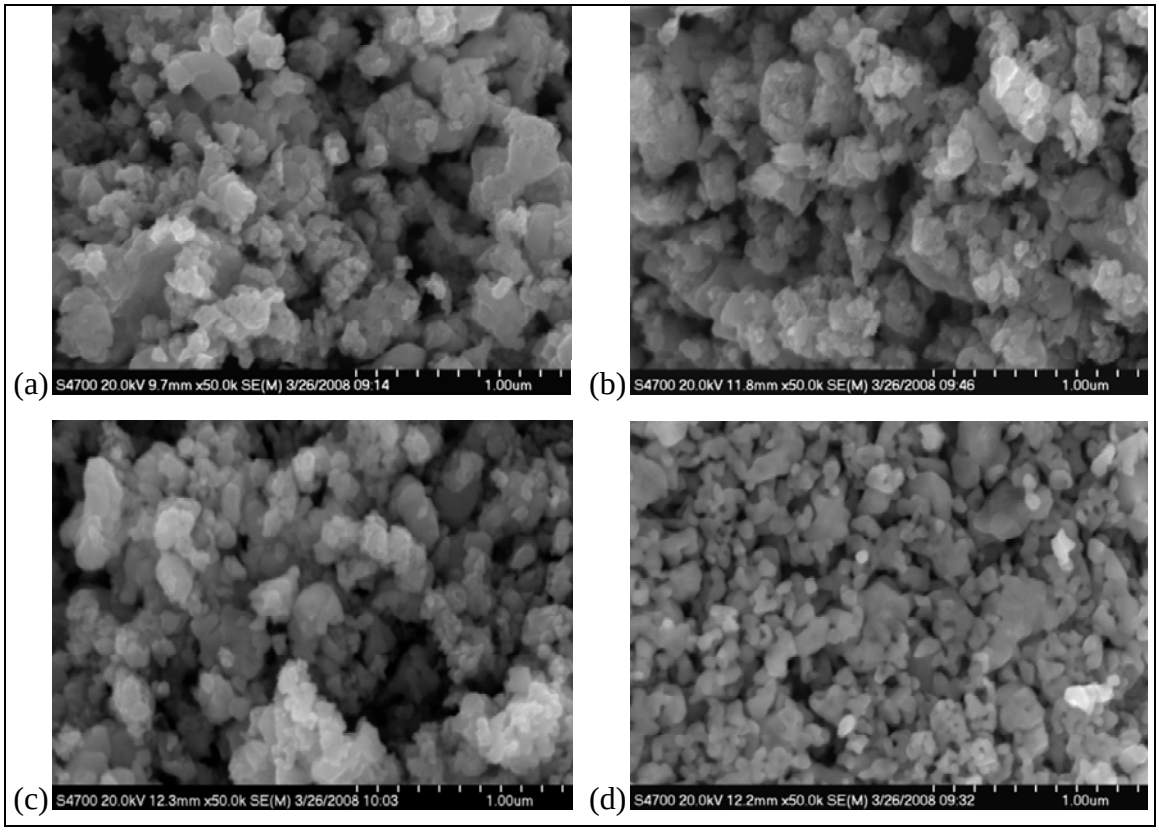


Figure 13. FESEM micrographs of hydrogen reduced compacts (a) unheated, (b) 650, (c) 750, and (d) 850 °C.

Based on these results, reduction under ultra-high purity (UHP) hydrogen with a dew point of –71 °C at 650 °C for 6 h and 20 min was found to produce a compact with the least amount of sintering when compared to an unreduced green body sample.

Results of density measurement for the tungsten powder are shown in table 5. In all of the conditions tested, the powder showed density values lower than that of pure tungsten (19.3 g/cm$^3$).

Table 5. Density of tungsten measured by helium pycnometry.

| Condition | Average Density (g/cm$^3$) | Standard Deviation (g/cm$^3$) |
|---|---|---|
| As-received | 16.9 | 0.02 |
| Baked | 16.48 | 0.06 |
| Milled and baked | 15.97 | 0.02 |

Initially, four samples of tungsten were consolidated to compare the effect of different starting powder conditions on the final sample. All samples were run in the P$^2$C apparatus under the same pulsing and consolidation conditions. Densities for these samples are shown in table 6. The powder for the first P$^2$C consolidation sample was milled and reduced using the ideal milling and reduction conditions as determined previously. However, rather than reducing the powder in the tube furnace as a pressed compact, the powder was loaded into a graphite die prior to reduction. The powder was pressed inside the die, the punches were removed, and the entire die was inserted into the reduction furnace. This was done to facilitate easier loading into the P$^2$C. After reduction in the tube furnace, the die was placed in the P$^2$C press and processed at 100 MPa and a die temperature of 1600 °C. The final density for the first sample was 16.96 g/cm$^3$ (87.9% theoretical density) with grain sizes as observed by FESEM varying between 1 and 10 µm (figure 14a). The sample also had tungsten oxide identified by EDS in the light gray phase present between the tungsten grains. The P$^2$C process was then repeated, this time with the powder reduction done in an alumina boat to allow for the tungsten powder to be spread out, providing a shorter diffusion path for the hydrogen and a better escape pathway for the water vapor formed. The resulting P$^2$C sample (figure 14b) still had grain sizes between 1 and 10 µm, as well as the presence of tungsten oxide, but it had a slight increase in density to 17.4 g/cm$^3$ (90.2% theoretical). The P$^2$C parameters were repeated using unreduced milled tungsten powder (figure 14c) and un-milled, unreduced powder (figure 14d). The respective densities were 16.58 (85.9% theoretical) and 16.37 g/cm$^3$ (84.8% theoretical). Both samples also had similar grain size, as well as tungsten oxide present at tungsten grain boundaries. The sample made with unmilled powder also appeared to contain more porosity and a less uniform microstructure, likely due to the presence of the large agglomerates which would normally be broken up with milling.

Table 6. Densities of $P^2C$ consolidated samples with varying starting powder conditions.

| Powder Conditions | Reduction Conditions | Density ($g/cm^3$) | Theoretical Density (%) | Oxygen (Weight-Percent) |
|---|---|---|---|---|
| Milled | Reduced in die at 650 °C for 380 min | 16.96 | 87.9 | NA |
| Milled | Reduced in boat at 650 °C for 380 min | 17.40 | 90.2 | 0.27 |
| Milled | Unreduced | 16.58 | 85.9 | 0.42 |
| Unmilled | Unreduced | 16.37 | 84.8 | 0.24 |

NA = not available.

Three of these consolidated samples were also sent for measurement of oxygen content via inert gas fusion. The weight percent oxygen measured for each sample is also shown in table 6. The consolidated sample of milled powder reduced in a boat prior to consolidation (90.2% dense) was found to have 0.27 weight-percent oxygen, while the unreduced, milled sample (85.9% dense) contained 0.42 weight-percent oxygen. However, the unreduced, unmilled powder (84.8% dense) sample contained 0.24 weight-percent oxygen. Based on these results, it appeared that the oxygen picked up by the powder during the milling step resulted in extra oxygen present in the consolidated sample even after reduction and consolidation. A more sophisticated milling procedure which disperses the tungsten powder in a solvent such as isopropanol prior to milling could help to prevent the addition of oxygen.

At this point, in an attempt to determine $P^2C$ processing conditions that would provide for samples with final grain size in the ultra-fine or nano regime, a series of lower temperature $P^2C$ runs were undertaken to attempt to reduce grain growth during consolidation. To facilitate faster sample production, milling and reduction of the powder prior to consolidation was discontinued until the desired grain size was achieved. Unreduced, un-milled powder was $P^2C$ processed at final temperatures of 1100, 1200, and 1300 °C using the same pulsing parameters and pressure as before. Density values for these samples are shown in table 7. FESEM micrographs are shown in figure 15. The 1100 °C sample was seen to retain the fine grain size (<100 nm) of the starting powder. However, the density of this sample was only 12.31 $g/cm^3$ (63.8% theoretical). At 1200 °C, the density of the consolidated sample was 16.54 $cm^3$ (85.7% theoretical), which is similar to what was achieved using 1600 °C. The grains size of this sample ranged from 200 to 500 nm. At 1300 °C, the sample density was 16.03 $cm^3$ (83.1% of theoretical) and the grains were slightly larger than the 1200 °C sample. It was decided to try reduction of the powder prior to $P^2C$ consolidation at 1200 °C to increase the final density of the samples while retaining the fine grain size.

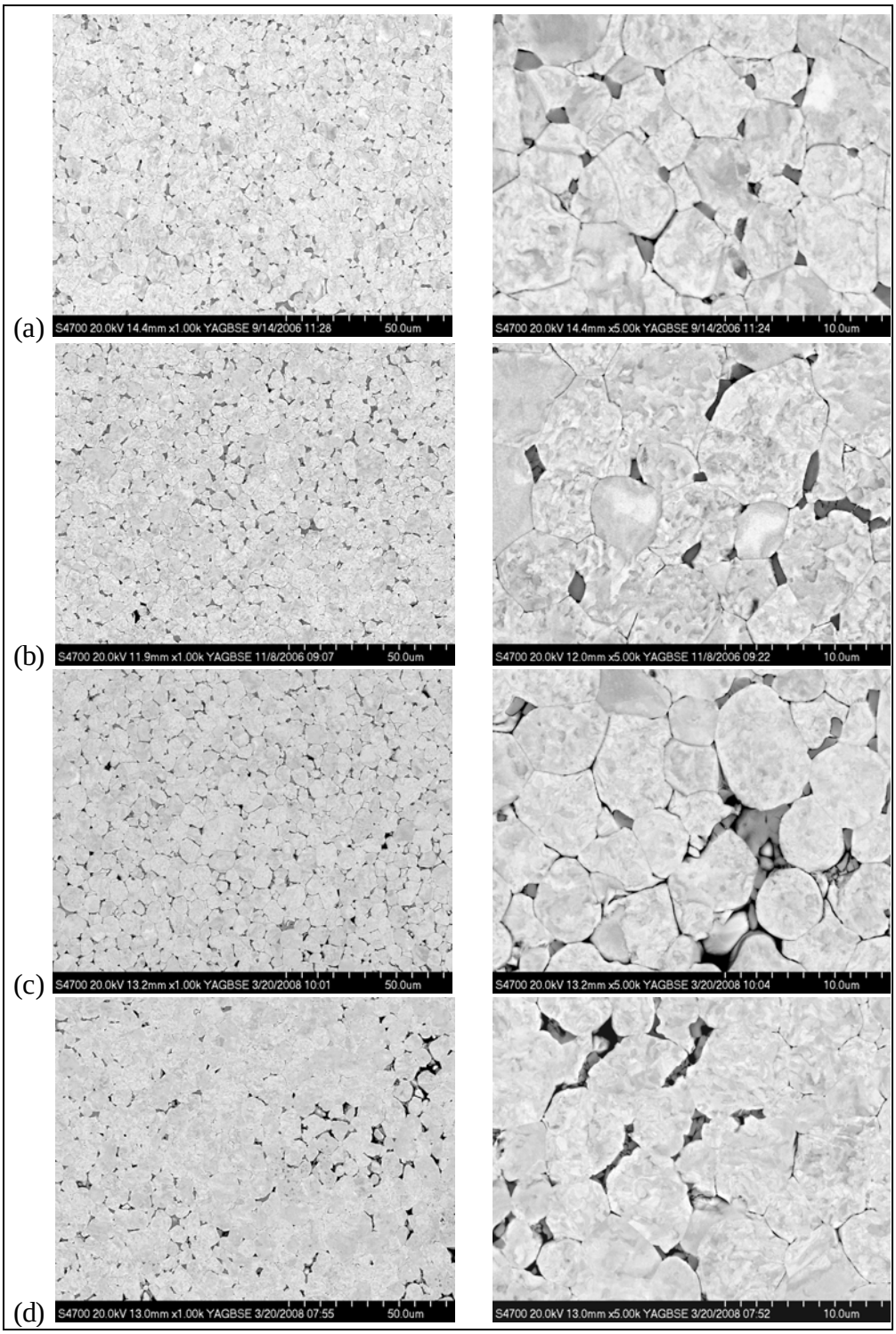


Figure 14. FESEM micrographs of $P^2C$ samples consolidated at 1600 °C and 100 MPa using (a) milled powder reduced in a graphite die, (b) milled powder reduced in an alumina boat, (c) unreduced milled powder, and (d) unreduced unmilled powder.

Table 7. Densities of $P^2C$ samples processed at lower temperatures.

| Powder Condition | Consolidation Temperature (°C) | Density ($g/cm^3$) | Theoretical Density (%) |
|---|---|---|---|
| Unmilled, unreduced | 1100 | 12.31 | 63.8 |
| Unmilled, unreduced | 1200 | 16.54 | 85.7 |
| Unmilled, unreduced | 1300 | 16.03 | 83.1 |
| Unmilled, reduced in $P^2C$ | 1200 | 15.44 | 80.0 |
| Unmilled, reduced in $P^2C$ | 1200 | 15.88 | 82.3 |

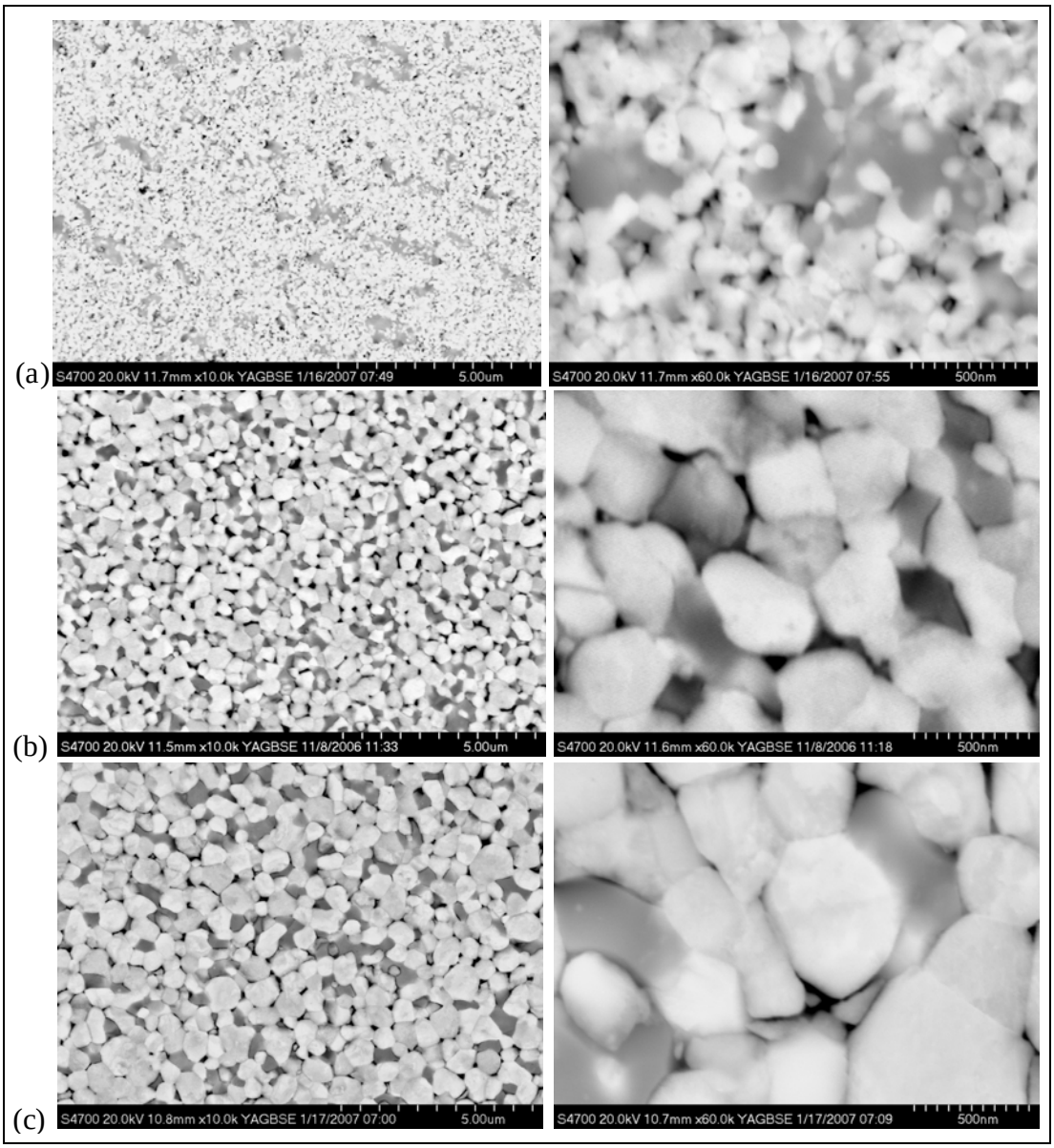


Figure 15. FESEM micrographs of $P^2C$ samples consolidated at (a) 1100, (b) 1200, and (c) 1300 °C.

However, when attempts were made to reduce the un-milled powder in a tube furnace under the previously-developed conditions of 650 °C for 6 h and 20 min, the samples spontaneously reacted to form tungsten oxide upon extraction from the furnace. It was unclear why the reduction parameters at 650 °C did not work as before. It is possible that, due to the powder being in the un-milled condition, the lower oxygen content in the initial powder resulted in a lower final oxide content and made the powder more reactive subsequent to the reduction step.

Due to these issues with reduction of the powder in the tube furnace, hydrogen reduction runs were performed in the $P^2C$ prior to consolidation. Two samples were run under identical consolidation conditions, both being reduced in the $P^2C$ chamber under hydrogen at 650 °C for 380 min prior to consolidation. Density values for these samples are also shown in table 7, and FESEM images of the microstructure of each sample can be seen in figure 16. Reduction in the $P^2C$ did not appear to have any significant effects on grain size, but did result in slightly lower densities than for the previous unreduced sample consolidated at 1200 °C. It is not clear why these samples had lower density values than the previous samples. It is possible that some partial sintering occurred during the reduction process, creating large agglomerates that hindered sintering during the final consolidation step.

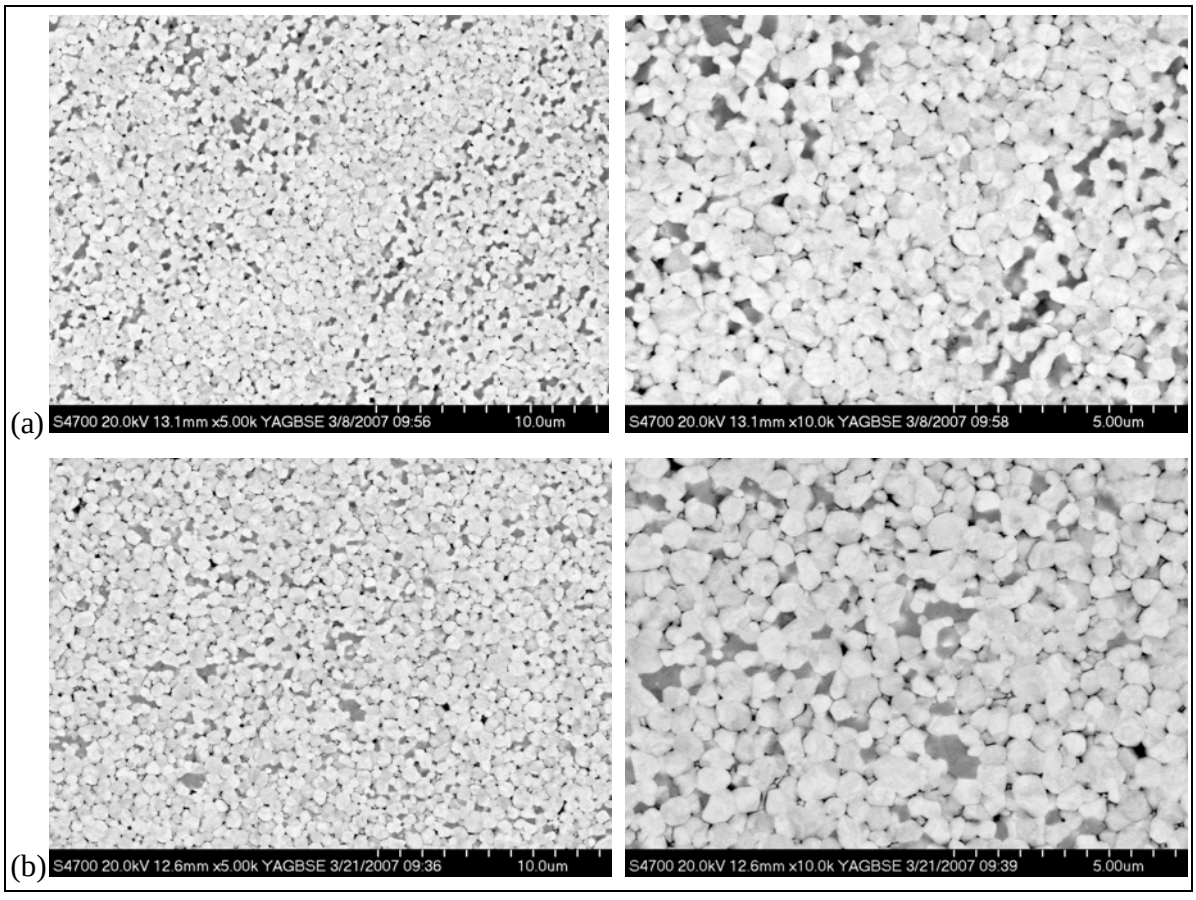


Figure 16. Samples reduced in $P^2C$ chamber prior to consolidation.

FESEM observation revealed that the samples reduced in the $P^2C$ were found to have some areas with porosity present, but little or no tungsten oxide (figure 17). The oxide free areas were always within 500 µm of the edge of the sample. Reexamination of previous $P^2C$ consolidated samples that were not subjected to a hydrogen environment in the chamber prior to consolidation also showed similar phenomena. Prior to the use of hydrogen, the standard industrial practice to reduce tungsten oxide to pure tungsten metal involved the use of carbon as a reducing agent (*8*). Thus, it seems probable that the oxide free zone is not a result of hydrogen reduction, but is formed due to contact between the tungsten powder compact and either the graphite die itself or carbonaceous vapors produced by the die during the $P^2C$ process. The samples reduced in the $P^2C$ may have had large oxide free areas because of the extra time that the graphite die was in contact with the tungsten powder at elevated temperatures.

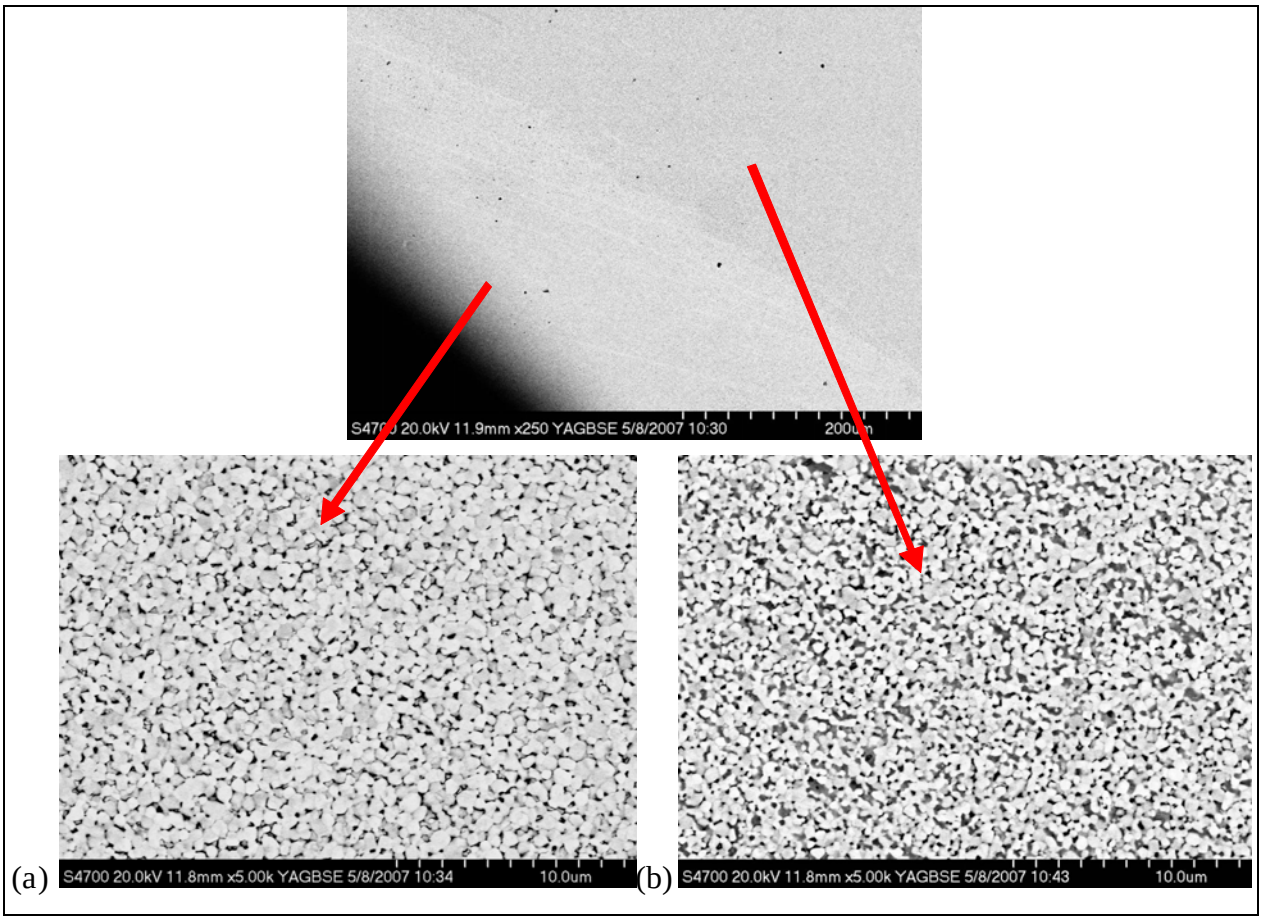


Figure 17. FESEM images showing an (a) oxide free zone and (b) oxide containing region in $P^2C$ consolidated samples.

## 4. Conclusions

The purpose of this study was to characterize a commercially available nano-tungsten powder and evaluate its behavior when consolidated using the Plasma Pressure Compaction ($P^2C$) method with the goal of achieving a fully dense sample with a final grain size in the nanocrystalline or ultra-fine grain regime. Characterization revealed a need for processing of the powder prior to consolidation. Mechanical milling was performed to reduce agglomeration of the nanoparticles, and hydrogen reduction of the powder prior to insertion into the $P^2C$ apparatus was introduced to reduce oxygen contamination. Milling was found to break up agglomerates and reduce the mean particle size of the powder, providing for a more uniform microstructure and an increase in the final density of the consolidated samples. The external hydrogen reduction process prior to $P^2C$ consolidation was shown to be capable of increasing the density of the samples, but the reduction step has yet to be effectively applied in-situ during $P^2C$ processing. Although it was possible to produce bulk samples with ultra-fine and nano-sized grains using the nano-scale powder, it was not possible to maintain the nanocrystallinity of the consolidated samples while achieving high density.

## 5. References


1. Magness, L. S.; Farrand, T. G. Deformation Behavior and its Relationship to the Penetration Performance of High Density Kinetic Energy Penetrator Materials. *Proceedings of the 17th Army Science Conference*, 1990, pp 149–165.

2. Cai, W. D.; Li, Y.; Dowding, R. J.; Mohamed, F. A.; Lavernia, E. J. A Review of Tungsten-Based Alloys as Kinetic Energy Penetrator Materials. *Reviews in Particulate Materials* **1995**, *3*, 71–132.

3. Wei, Q.; Jiao, T.; Ramesh, K. T.; Ma, E.; Kecskes, L. J.; Magness, L.; Dowding, R.; Kazykhanov, V. U.; Valiev, R. Z. Mechanical Behavior and Dynamic Failure of High-Strength Ultrafine Grained Tungsten under Uniaxial Compression. *Acta Materialia* **2006**, *54* (1), 77–87.

4. Wei, Q.; Zhang, H. T.; Schuster, B.; Ramesh, K. T.; Ma, E.; Valiev, R. Z.; Kecskes, L. J.; Cho, K. C.; Dowding, R. J.; Magness, L. Microstructure and Mechanical Properties of Super-Strong Nanocrystalline Tungsten by High-Pressure Torsion. *Acta Materialia* **2006**, *54* (15), 4079–4089.

5. Cho, K.; Kellogg, F.; Klotz, B.; Dowding, R. Plasma Pressure Compaction ($P^2C$) of Submicron Size Tungsten Powder. *Proceedings of the International Conference on Tungsten, Refractory, and Hardmetals VI*, 2006.

6. Cho, K.; Woodman, R.; Klotz B.; Dowding, R. Plasma Pressure Compaction of Tungsten Powders. *Materials and Manufacturing Processes* **2004**, *19* (4), 619–630.

7. McWilliams, B.; Zavaliangos, A.; Cho, K. C.; Dowding, R. J. The Modeling of Electric-Current-Assisted Sintering to Produce Bulk Nanocrystalline Tungsten. *JOM: Journal of the Minerals, Materials, and Metals Society* **2006**, *58* (4), 67–71.

8. Yih, S.; Wang, C. *Tungsten: Sources, Metallurgy, Properties, and Applications*; Plenum Press: New York, 1979; p 137.

NO. OF
COPIES ORGANIZATION

1 (PDF only) DEFENSE TECHNICAL INFORMATION CTR
DTIC OCA
8725 JOHN J KINGMAN RD
STE 0944
FORT BELVOIR VA 22060-6218

1 DIRECTOR
US ARMY RESEARCH LAB
IMNE ALC HRR
2800 POWDER MILL RD
ADELPHI MD 20783-1197

1 DIRECTOR
US ARMY RESEARCH LAB
RDRL CIM L
2800 POWDER MILL RD
ADELPHI MD 20783-1197

1 DIRECTOR
US ARMY RESEARCH LAB
RDRL CIM P
2800 POWDER MILL RD
ADELPHI MD 20783-1197

ABERDEEN PROVING GROUND

1 DIR USARL
RDRL CIM G (BLDG 4600)

NO. OF COPIES ORGANIZATION

5 DIRECTOR
US ARMY RSRCH LAB
RDRL WMM B
A ABRAHAMIAN
M BERMAN
A FRYDMAN
R KARGUS
T LI
2800 POWDER MILL RD
ADELPHI MD 20783-1197

1 COMMANDER
US ARMY TACOM ARDEC
AMSRD AAR EM
J HEDDERICH
PICATINNY ARSENAL NJ 07806-5000

1 COMMANDER
US ARMY TACOM ARDEC
AMSRD AAR EMT
B MACHAK BLDG B1
PICATINNY ARSENAL NJ 07806-5000

3 COMMANDER
US ARMY TACOM ARDEC
AMSRD AAR AEP E
S GROESCHLER
J LEE
J VEGA
BLDG 94
PICATINNY ARSENAL NJ 07806-5000

1 COMMANDER
US ARMY TACOM ARDEC
AMSRD AAR AEM J
G FLEMING BLDG 65N
PICATINNY ARSENAL NJ 07806-5000

2 COMMANDER
US ARMY TACOM ARDEC
AMSRD AAR EBM
R CARR
W SHARPE
BLDG 1
PICATINNY ARSENAL NJ 07806-5000

3 COMMANDER
US ARMY TACOM ARDEC
SFAE AMO MAS LC
R DARCY
R JOINSON
D RIGOGLIOSO
BLDG 354
PICATINNY ARSENAL NJ 07806-5000

NO. OF COPIES ORGANIZATION

1 COMMANDER
US ARMY TACOM ARDEC
AMSRD AAR AEM L
D VO
BLDG 65 S
PICATINNY ARSENAL NJ 07806-5000

2 COMMANDER
US ARMY TACOM ARDEC
AMSRD AAR AEM
S MUSALLI
M LUCIANO
BLDG 65S
PICATINNY ARSENAL NJ 07806-5000

2 COMMANDER
US ARMY TACOM ARDEC
AMSRD AAR AEM
A VELLA
J LUTZ
BLDG 354
PICATINNY ARSENAL NJ 07806-5000

1 COMMANDER
US ARMY TACOM ARDEC
AMSRD AAR AEM
T LOUZEIRO
BLDG 65
PICATINNY ARSENAL NJ 07806-5000

1 COMMANDER
US ARMY TACOM ARDEC
AMSRD AAR AEM
L MANOLE
BLDG 65N
PICATINNY ARSENAL NJ 07806-5000

2 COMMANDER
US ARMY TACOM ARDEC
AMSRD AAR AEE P
D KAPOOR
S KERWIEN
BLDG 25
PICATINNY ARSENAL NJ 07806-5000

1 COMMANDER
US ARMY TACOM ARDEC
AMSRD AAR AIP
M LOS
BLDG 1
PICATINNY ARSENAL NJ 07806-5000

NO. OF COPIES ORGANIZATION

2 SFSJM CDL
AMMUN TEAM
AMSIO SMT
R CRAWFORD
W HARRIS
1 ROCK ISLAND ARSENAL
ROCK ISLAND IL 61299-6000

3 BENET LABS
AMSTA AR CCB
M SOJA
E KATHE
P WHEELER
WATERVLIET NY 12189-4050

5 BENET LABS
AMSTA CCB R
S SOPOK
E HYLAND
D CRAYON
R DILLON
G VIGILANTE
WATERVLIET NY 12189-4050

1 US ARMY TARDEC
AMSRD TAR R
D TEMPLETON
6501 E 11 MILE RD MS 263
WARREN MI 48397-5000

1 PEO GROUND COMBAT SYS
SFAE GCS BCT/MS 325
M RYZYI
6501 ELEVEN MILE RD
WARREN MI 48397-5000

1 USA RDECOM
AMSRD AMR AE F T
J CHANG
BLDG 488 B247
REDSTONE ARSENAL AL 35898

1 USA RDECOM
AMSRD AMR AE F A
M ROGERS
BLDG 4488 B244
REDSTONE ARSENAL AL 35898

2 USA RDECOM
AMSRD AMR AE F M
G LIU
R MCFARLAND
BLDG 4488 B272
REDSTONE ARSENAL AL 35898

NO. OF COPIES ORGANIZATION

4 US ARMY RSRCH OFC
J PRATER
D STEPP
D KISEROW
L WALKER
PO BOX 12211
RESEARCH TRIANGLE PARK NC
27709-2211

1 COMMANDER
US ARMY TACOM ARDEC
AMSTA AR CCL B
J MIDDLETON
BLDG 65N
PICATINNY ARSENAL NJ 07806-5000

1 COMMANDER
US ARMY TACOM ARDEC
ASIC PRGM INTEGRATION OFC
J RESCH
BLDG 1
PICATINNY ARSENAL NJ 07806-5000

1 COMMANDER
US ARMY TACOM ARDEC
AMSRD AAR AEW M(D)
M MINISI
BLDG 65 N
PICATINNY ARSENAL NJ 07806-5000

1 US ARMY TACOM ARDEC
AMSRD AR CCL C
S SPICKERT-FULTON
BLDG 65 N
PICATINNY ARSENAL NJ 07806-5000

4 PM ARMS
SFAE AMO MAS SMC
R KOWALSKI
F HANZL
P RIGGS
M BULTER
BLDG 354
PICATINNY ARSENAL NJ 07806-5000

1 PM ARMS
SFAE AMO MAS MC
BLDG 354
PICATINNY ARSENAL NJ 07806-5000

1 DARPA
S WAX
3701 N FAIRFAX DR
ARLINGTON VA 22203-1714

NO. OF COPIES ORGANIZATION

1 DIRECTOR
NGIC
IANG TMT
D QUEHEILALT
2055 BOULDERS RD
CHARLOTTESVILLE VA
22091-5391

2 GENERAL DYNAMICS OTS
FLINCHBAUGH DIV
K LINDE
G KURZIK
PO BOX 127
RED LION PA 17356

1 DIRECTOR
US ARMY RESEARCH LAB
RDRL CI
2800 POWDER MILL RD
ADELPHI MD 20783-1197

ABERDEEN PROVING GROUND

1 US ARMY ATC
CSTE DTC AT AD I
W FRAZER
400 COLLERAN RD
APG MD 21005-5059

46 DIR USARL
RDRL LOA F
M ADAMSON
RDRL WM
L BURTON
J SMITH
S KARNA
J MCCAULEY
P PLOSTINS
RDRL WMB D
P CONROYP
RDRL WML
M ZOLTOSKI
J NEWILL
RDRL WML A
W OBERLE
RDRL WML E
P WEINACHT
RDRL WML F
D LYON
RDRL WML G
W DRYSDALE
RDRL WMM
H MAUPIN
J BEATTY

NO. OF COPIES ORGANIZATION

R DOWDING
RDRL WMM A
M VANLANDINGHAM
RDRL WMM B
R CARTER
W DE ROSSET
L KECSKES
E KLIER
D SNOHA
B KLOTZ
J SWAB
RDRL WMM C
M MAHER
W SPURGEON
F KELLOGG
RDRL WMM D
E CHIN
J ADAMS
K CHO
RDRL WMT
P BAKER
RDRL WMT A
S SCHOENFELD
D HACKBARTH
RDRL WMT B
R GUPTA
B MCANDREW
RDRL WMT C
T BJERKE
G BOYCE
K KIMSEY
L MAGNESS
B SCHUSTER
B SORENSEN
R SUMMERS
B WALTERS
RDRL WMT D
D CASEM
T WEERASOORIYA
RDRL WMT E
B RINGERS

INTENTIONALLY LEFT BLANK.